Int. J. Electrochem. Sci., 7 **(2012)** 8940 - 8957

International Journal of
ELECTROCHEMICAL
SCIENCE
www.electrochemsci.org

Electrocatalytic Properties of Bimetallic Surfaces for the Oxygen Reduction Reaction

A.Ezeta-Mejía[1], *O.Solorza-Feria*[2], *H.J.Dorantes-Rosales*[1], *J.M.Hallen López*[1], *E.M.Arce-Estrada*[1,*]

[1] Instituto Politécnico Nacional. ESIQIE. Depto. de Ingeniería en Metalurgia y Materiales, UPALM Ed. 7, 07738, México D.F., México.
[2]Centro de Investigación y de Estudios Avanzados del IPN. Depto. de Química, A. Postal 14-740, 07360 México D.F., México
[*]e-mail: earce@ipn.mx

Received: 20 February 2012 / *Accepted:* 14 March 2012 / *Published:* 1 September 2012

The physical characterization of nanocrystalline RuM (M=Se,Mo,W,Sn) prepared by mechanical alloying (MA) technique at different milling times shows the formation of mixture of phases ($FeSe_2$, Fe_2O_3, Ru and Se), solid solution (Ru and Mo), Ru_3W_2 and $RuSn_2$ intermetallic compounds with nanocrystalline nature of 2 to 20 nm in size. The activity of the nanocatalysts supported on Vulcan carbon was investigated by rotating disk electrode for the oxygen reduction reaction (ORR) in 0.5 H_2SO_4. Results reveal improved specific activities toward the ORR with multielectron transfer process (n=4e-) to water formation. The effect of temperature on the ORR kinetics was also investigated, concluding that the Tafel slope is temperature invariant while the transfer coefficient shows important dependence.

Keywords: Electrocatalyst; Oxygen reduction; Ruthenium; Mechanical alloying

1. INTRODUCTION

Electrocatalyst nanotechnology is an interesting area of research which opens up new possibilities for applications of a diversity of synthesized novel materials for the renewable energy sector. Most of the research in nanomaterials is performed on dispersed or supported powders which contains nanoparticles. Oxygen reduction reaction (ORR) has been intensively investigated from a fundamental as well as from a practical point of view. The impact of the oxygen reduction reaction on fuel cells, metal-air batteries and materials degradation as oxygen-consuming cathodes or in water electrolysis as oxygen-electrogenerator anode put in evidence its importance [1-2]. There have been great efforts to develop novel, inexpensive, more active and stable nanocatalysts for the oxygen reduction reaction because one of mayor problems is the irreversible and its large overpotential required to reaction occur, it leads for example, to a significant loss on efficiency of the fuel cells. ORR in platinum and platinum-based alloy electrodes has been widely studied because low temperature fuel cell systems present a promising method of energy production [3-4] and more used because of their high activity and stability in acid media [4]. Due the capital cost of platinum, it is required to develop novels highly active and stable electrocatalysts for ORR. Considering that the fuel cell efficiency is related with the catalyst activity, i.e., the size of its particles, density, geometry, composition, dispersion and interaction with the support, it is of paramount important to control these factors during the synthesis process. In the last years, research has been fundamental focused on the development of two types of catalyst: catalysts based on heat treated carbon-supported iron or cobalt compounds, whose active centers most probably consist of single metal centers coordinated by nitrogen and carbon [5-7] or related to the preparation of carbon supported transition-metal nanoparticles (mainly ruthenium), which surface is modified by a chalcogenide (i.e., selenium) or clusters-like structures [8-12]. On the other hand, various metal phtalocyanines and porphyrins [13] and metal oxides [14] have been reported to exhibit relevant ORR activity. Also, it was found that carbon supported ruthenium nanoparticles also catalyze the ORR [15-17] in acid media, but with limited activity that does not represent a viable alternative for technical applications. Recently, some authors has been put in evidence that surface modification of ruthenium nanoparticles with selenium [17-20] or molybdenum [17,21], tin [22] and tungsten [23] alters its electrochemical properties and enhances the activity towards the oxygen reduction reaction.

The main interest of this work is to study the catalytic activity of RuM (M = Se,Mo,W,Sn) catalysts, prepared by mechanical alloying to produce bimetallic nanoparticle materials in order to enhance the ruthenium-based catalytic activity compared to ruthenium alone. The effect of temperature on the ORR kinetic constitutes also part of this work.

2. EXPERIMENTAL PROCEDURE

2.1 Chemicals and reagents

Ru, Se, Mo, W and Sn powders were reagents from Aldrich with 99.9 % nominal purity and < 74 μm, < 149 μm, < 10 μm, < 10 μm and < 44 μm particle size, respectively and H_2SO_4 of high purity was obtained from Aldrich.

2.2 Synthesis of RuM powders by AM

Preparation of the catalytic powders (RuM) was achieved by the mechanical alloying (MA) technique. Ru and M (Se, Mo, W, Sn) with a ratio of 1:1, were introduced in a SPEX 8000 high-energy ball mill using a stainless steel vials and steel balls to RuSe and RuMo and zirconium balls to RuW and RuSn, with a ball to powder ratio of 4:1. The surfactant agent was 1 *wt %* of methanol to RuSe and RuMo and 1 *wt %* of isopropanol to RuW and RuSn, under inert atmosphere (argon, high purity). Vials were rotated at 1200 rpm for a period of 20 and 40 h.

2.3 Physical characterization

The phase identification of the MA bimetallic powders was performed in the X-ray Diffractometer (XRD) for powders using a D8 Focus Bruker AXS equipment with Cu Kα radiation. The surface morphology was examined using a scanning electron microscope (SEM) in a JEOL JSM-6300 operated at 20 kV equipped with an energy dispersive spectrometer, and the particle size determined from transmission electron microscopy (TEM) analysis in a JEOL 2000-FXII operated at 200 kV.

The calculation to estimate the crystallite size of the dispersed RuM catalyst was based on the broadening of RuM reflection peaks, following the Scherrer´s equation [22].

$$D = \frac{k\lambda}{B\cos\theta} \qquad (1)$$

Where D is the mean particle size in $\mathring{A}$, k is a coefficient taken here as 0.9, λ the wavelength of the X-rays used (1.540546 Å), B the width of the diffraction peak at half height in radians, and θ the angle at the position of the peak maximum.

2.4 Electrode preparation for RDE study and electrochemical set-up

Rotating disk electrode, RDE, technique was used for electrochemical characterization. A vitreous carbon rod with a 5 mm diameter (cross-sectional area of 0.1963 cm^2) was inserted under pressure within a cylindrical Teflon support. The exposed surface of vitreous carbon was grinded with 400 and 600 emery papers to adhere the electrocatalyst ink. The ink was prepared by mixing 1 mg of each synthesized electrocatalysts with 0.4 mg of Vulcan carbon, 12 μl of Nafion® and 0.3 ml of ethanol. The mixture was set under ultrasonic treatment to form a homogeneous suspension; 5 μl of suspension were placed by means of a micropipette on the vitreous carbon support, forming a homogeneous thin film. The prepared electrode was dried for 24 h at room temperature.

2.5 Experimental setup

The electrochemical measurements were performed in a conventional three-electrode cell (50 ml). A platinum stick was used as the counter electrode. The reference electrode was a saturated calomel electrode (SCE) that was inserted separately in a compartment lodging of a Luggin capillary and was place outside of the cell, kept at room temperature. All potentials were referred to the normal hydrogen electrode (NHE). A 0.5 M H_2SO_4 aqueous solution was used as electrolyte, prepared with deionized water (18.6 MΩcm). Prior to the electrochemical assessment and surface electrode activation of the working electrode, the acid electrolyte was degassed with nitrogen of high purity. Thereafter, the acid electrolyte was saturated with pure oxygen and maintained on the electrolyte surface during the electrochemical experiments. The temperature of the cell was controlled by a thermostat (PolyScience) from 293 to 333 K. The Cyclic Voltammetry (CV) and the Rotating Disk Electrode (RDE) studies were performed with a potenciostat/galvanostat Autolab 30 and an EG&G PAR, model 636 rotation speed controller. The cyclic voltammetry was performed in oxygen free electrolyte from open circuit potential at a v = 50 mVs^{-1} for 40 cycles, enough time to reach stable voltammograms. Hydrodynamic experiments were recorded in the performed in the O_2 saturated electrolyte, in the range of rotation rate of 100-1600 rpm at a v = 5 mVs^{-1}.

3. RESULTS AND DISCUSSIONS

3.1 Physicochemical characterization results

3.1.1 X-Ray Diffraction

Table 1. Phases and crystallite size determined by Scherrer´s equation of the electrocatalysts produced by mechanical milling.

ELECTROCATALYSTS MILLING TIME	PHASES	CRYSTALLITE SIZE (nm)
Ru-Se 20 h	Ru	2-5
	Se	4-12
Ru-Se 40 h	Ru	10-20
	Se	4-7
	Fe_2O_3	6-11
	$FeSe_2$	4-9
Ru-Mo 20 h	Ru	4-11
Ru-Mo 40 h	Ru	3-13
Ru-W 20 h	Ru	7-9
	W	3-8
Ru-W 40 h	Ru_3W_2	2-6
Ru-Sn 20 h	Ru	6-20
	Sn	7-25
	$RuSn_2$	5-9
Ru-Sn 40 h	Ru	4-5
	$RuSn_2$	3-13

X-ray diffraction patterns of (A) RuSe, (B) RuMo, (C) RuW and (D) RuSn powder mixture at 0, 20 and 40 h of milling, are shown in Figure 1. It is observed at 0 h of milling in all patterns, a well defined diffraction peaks corresponding to pure phase to each element. The X-ray diffraction patterns of RuSe to 20 h of milling time, shows a slight displacement of Ru peaks, towards lower values new peaks begin to appear in different positions. To 40 h of milling time, it is observed the formation of homogeneous new phases formed with Fe, Se and oxygen, such as $FeSe_2$ and Fe_2O_3, mainly formed in

2θ between 20° and 65º, and several peaks of Ru and one peak of Se. In this material, Se has a greater affinity with Fe (came from the wear of the container and milling balls, inherent to the mechanical alloying process) and $FeSe_2$ is forming and Ru appears free. These phases were determined by EVA V1.02 software from Bruker. X-ray diffraction pattern of RuMo to 20 h of milling time shows that the Mo peaks disappeared which indicates that the Mo atoms entered Ru lattice. Peak displacement toward lower 2θ values, indicates the formation of a solid solution.

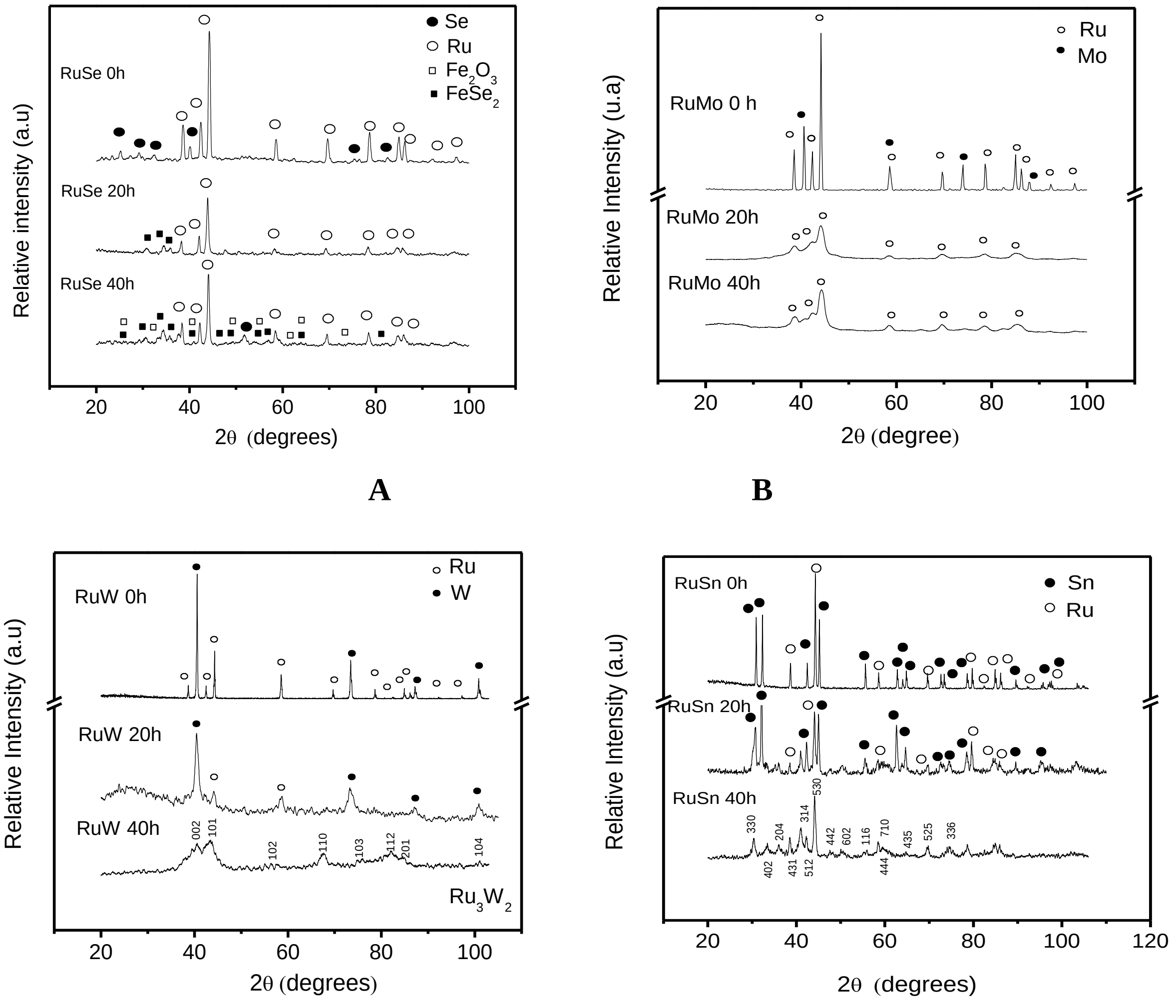

A B

C D

Figure 1. XRD patterns: (A) RuSe, (B) RuMo, (C) RuW, (D) RuSn.

In the RuW, X- ray diffraction patterns showed that to 20 h of milling time, all the Ru peaks disappear and for 40 h of milling time some new peaks appear corresponding to Ru_3W_2 intermetallic compound, identified by EVA V1.02 software. X-ray diffraction pattern of RuSn to 20 h, shows a decrease Ru and Sn peaks intensity and to 40 h of milling, new peaks appear corresponding to $RuSn_2$ intermetallic compound also identified by EVA V1.02. In all systems broad peaks are observed with lower intensity due to the reduction of crystallite size as a result of mechanical milling. The crystallite size was determined by Scherrer´s equation [24] and these results are reported in Table 1. In the RuSe y RuMo catalysts a growth in the crystallite size between 20 and 40 h of milling time is observed associated to an increase in lattice parameter by incorporation of iron atoms to the crystalline structure of these systems. The crystallite size in the RuW catalyst decreased to 40 h milling time due to hardness and brittleness of the Ru and W causing continuous particle fracture. To 20 and 40 h of milling in the RuSn a regular size is observed because the Sn is very ductile and only deform without breaking.

3.1.2 Scanning Electron Microscopy

At the early stages of milling, the components get flattened shapes which have been attributed to a micro-forging process [25].

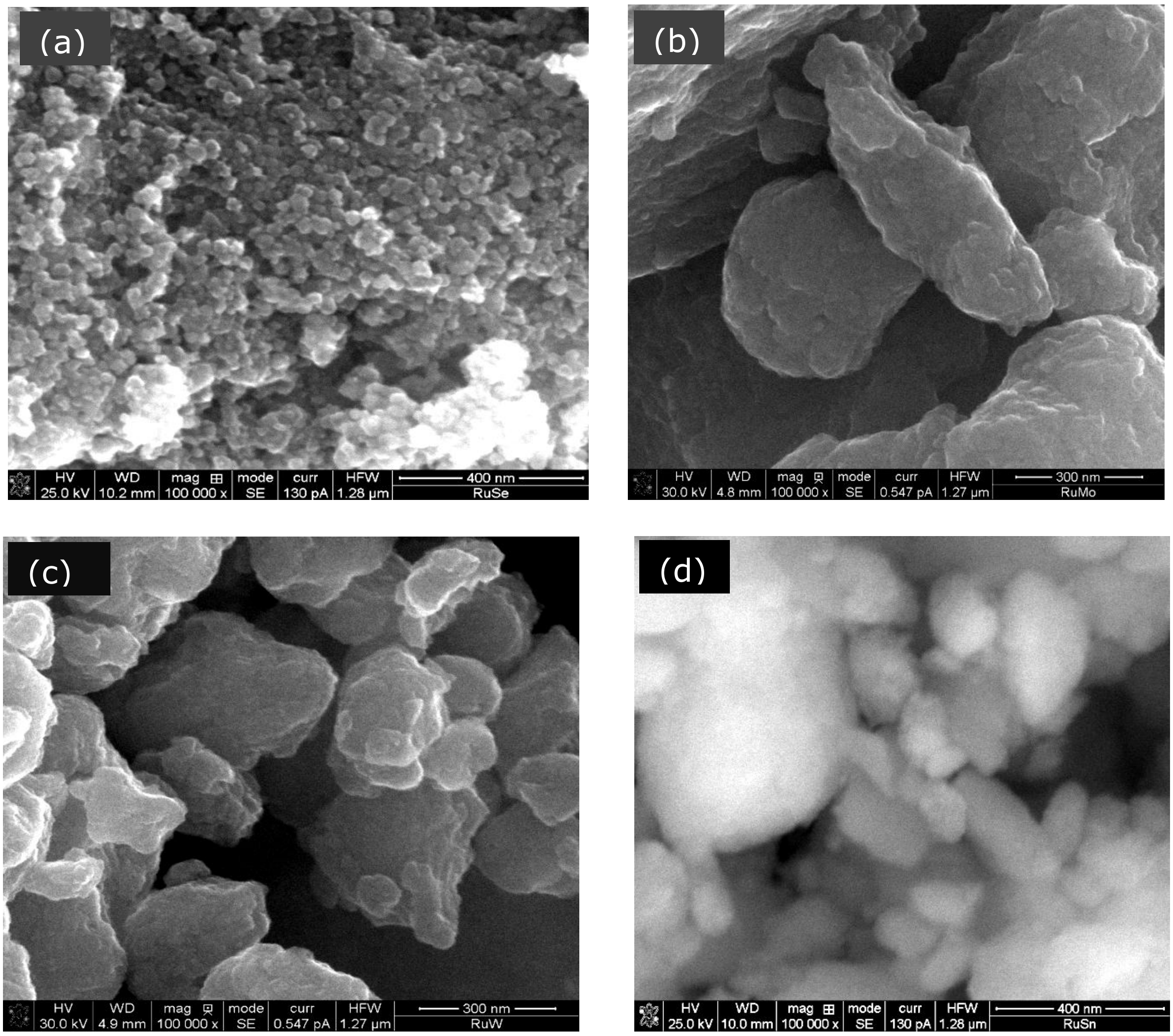

Figure 2. SEM micrographs of as synthesized particles of a) RuSe, b) RuMo, c) RuW, d) RuSn at 100 000X.

Figure 2 shows SEM micrographs for (a) RuSe, (b) RuMo, (c) RuW, (d) RuSn catalyst after 40 h of milling. In these micrographs it is observed agglomerates between 7-22 µm and 12-30 µm for RuSe and RuMo, respectively, formed by numerous granular morphology particles with sizes between 9–20 µm and 1-3 µm; these particles sizes are still much larger than the calculated crystallite size (~14nm), indicating that the particles are nanocrystalline as commonly reported for metallic materials produces by mechanical alloying [26]. The RuW and RuSn catalysts shows agglomerated particles with irregular morphology of 8-23 µm and 10-25 µm, respectively, formed by dispersed particles of 4-8 µm and 3-10 µm, in that order.

3.1.3 Transmission Electron Microscopy

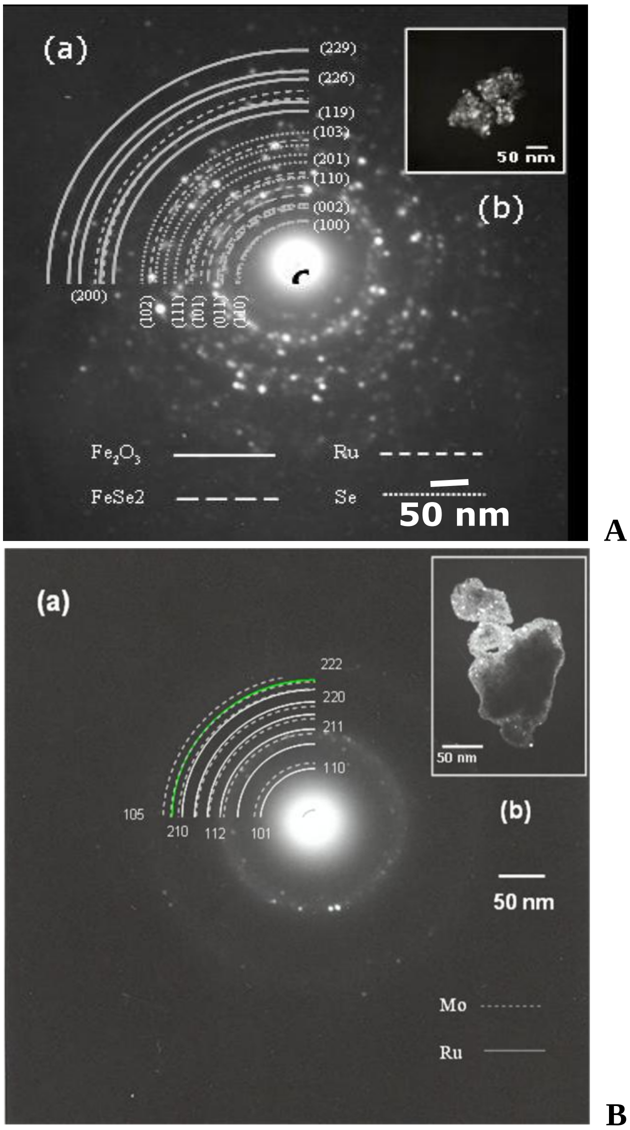

Figure 3. (a) Selected area electron diffraction patterns and (b) TEM dark field image: (A) RuSe, (B) RuMo electrocatalysts to 40 h of milling.

Figure 3 shows the TEM images obtained for the (A) RuSe and (B) RuMo catalysts milled for 40 h where a heavily agglomerate material is observed by SEM in both catalysts. These agglomerates are formed of nano-sized crystallites with a size about 7-30 nm for RuSe and 2-20 nm for RuMo. Then, the milling process induced the formation of nanometric grain size [27]. The indexed selected area of electron diffraction pattern confirmed the presence of different phases for RuSe and a solid solution for RuMo, determined by XRD. For RuW and RuSn catalysts nano-sized crystallites of about 2-6 nm and 3-13 nm, respectively were observed, and the indexed electron diffraction pattern, corresponding to Ru_3W_2 and $RuSn_2$ intermetallic compounds.

3.2 Electrochemical evaluation results

3.2.1 Electrochemical study of oxygen reduction reaction

The activation process is required to restructure the materials electrode surface at atomic scale in order to enhance the electrocatalytic properties by removing impurities and adsorbed molecular oxygen on the electrode surface. The reported current density is referred to the geometric electrode surface.

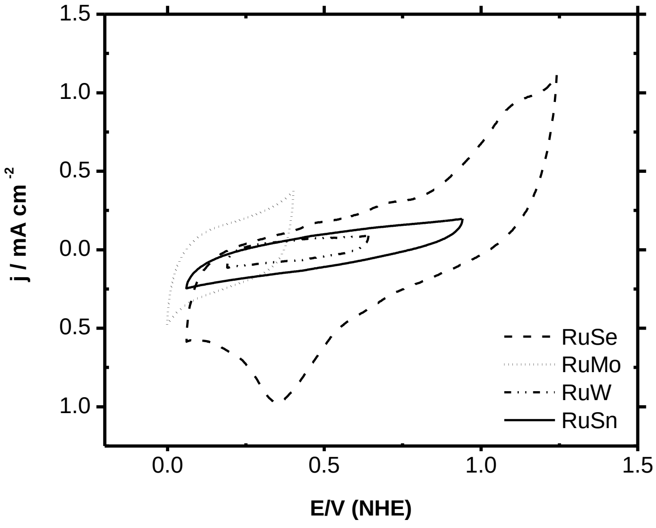

Figure 4. Cyclic voltammogram of RuSe, RuMo, RuW and RuSn electrocatalysts in H_2SO_4 0.5 M. and a scan rate of 50 mV s^{-1}.

The electrodes activation was performed by cyclic voltammetry in an oxygen free 0.5 M H_2SO_4 at scan rate of 50 mVs^{-1} for 40 cycles. Only catalytic activity of catalysts milling for 40h is presented, because this time of grinding was enough to obtain the best electrocatalytic responses. Cyclic voltammograms of RuSe, RuMo, RuSn and RuW are shown in Figure 4, it is observed the characteristic response of each system in the potentials range studied. RuSe catalysts in the range 0.25 - 0.45 V/NHE, shows a peak in the negative scan which is accounted for the reduction of a ruthenium surface oxide film. The broad peak indicates higher catalyst reducibility, probably caused by changes in the oxide coverage on the electrode surface. This is associated to the formation of mixed oxygen-selenium coverage of the ruthenium particles or to a catalytic influence of selenium on the ruthenium reducibility [28]. In the region 0.4 - 0.8 V an increasing anodic current is observed caused by overlapping of two stages of the ruthenium surface oxidation (Ru(0) to Ru(I) and Ru(II)), as suggested by Conway *et. al.* [29], while the other catalysts no presented significant redox peaks.

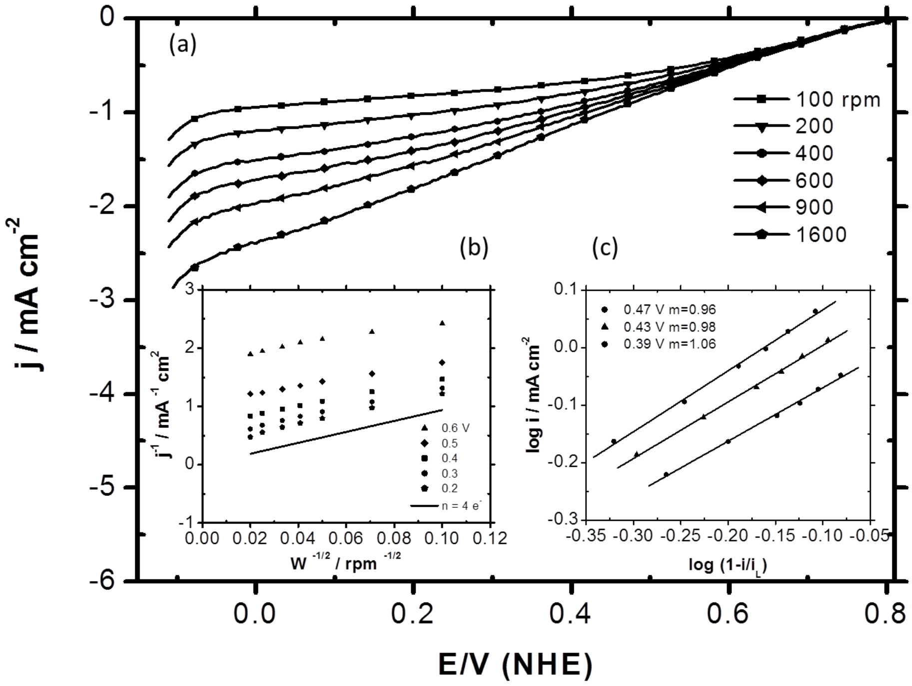

Figure 5. Current potential curves for the molecular oxygen reduction reaction on RuSe electrode in O_2 saturated 0.5M H_2SO_4 at 20°C. Inset b) Koutecky Levich plots represented in experimental and theoretical slopes and c) reaction order determination.

Figure 5, shows the polarization curves at different rotation rates of RuSe catalysts with Vulcan carbon powder dispersed into a Nafion film coated on a vitreous carbon, tested under oxygen saturated 0.5 M H_2SO_4 solution at 20°C, recorded from the open circuit potential to - 0.1 V/NHE. To RuSe catalysts, well defined kinetic currents are observed from 0.8 to 0.65 V/NHE, and mixed-diffusion limiting currents from 0.65 to -0.1 V/NHE, so the process is controlled by both charge transfer and mass transport processes. There is a dependence of the current density with the rotation rate as a consequence of the oxygen diffusion through the electrode surface. Comparing electrochemical responses of RuSe 20h and 40 h of milling, it is observed that at 40 h, the polarization curves present better mixed control zones and higher current density, due to the optimum particle size as well as the high concentration of Fe, obtained from the mechanical alloying process. Figure 6 shows RuMo polarization curves, where kinetic control between 0.70V and 0.60 V/NHE is observed; mixed control from 0.60V to 0.35 V/NHE and diffusion limiting currents from 0.60 to 0.35 V/NHE. Kinetic and diffusion limited currents in this material are well defined in the range of the electron transfer and mass transport zone due to the existence of a uniform distribution of electrocatalytic sites on the electrode surface [30], promoting a better electrocatalytic activity of this material. Compared RuMo 20 h and 40 h milling, at 20 h, there is a quasi-diffusion current from 0.5 to -0.096 V/NHE.

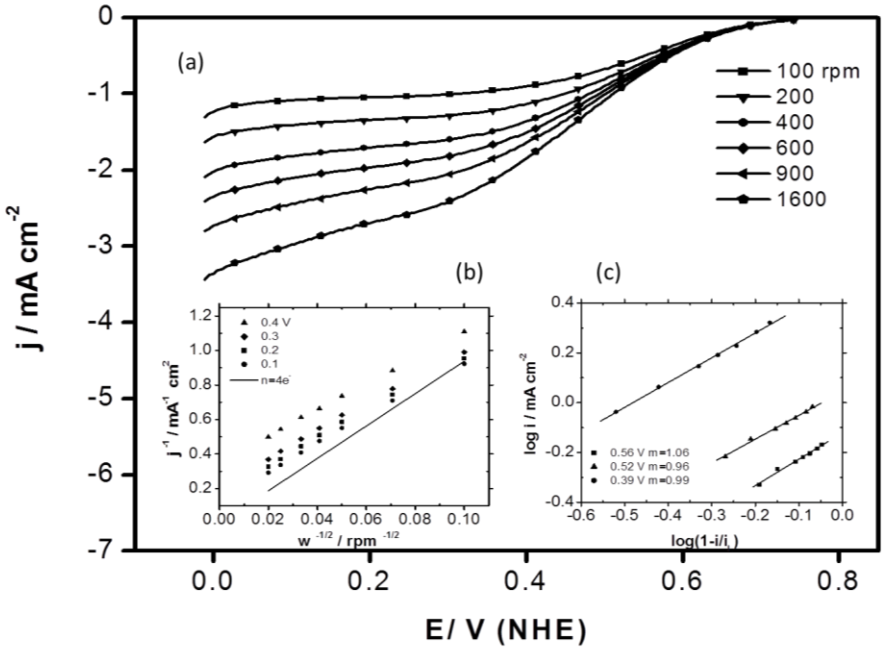

Figure 6. Current potential curves for the molecular oxygen reduction reaction for RuMo electrode in O_2 saturated 0.5M H_2SO_4 at 20°C. Inset b) Koutecky Levich plots represented in experimental and theoretical slopes and c) reaction order determination.

RuW and RuSn at 20 and 40 h milling not presented appreciable electrocatalytic activity towards ORR. At 40 h of milling in both catalysts, the activity increases but not enough to be considered as a candidate electrocatalysts for the ORR. With RuW, not electrocatalytic activity was observed, due probably to the small crystallite size, producing agglomeration of particles with decreasing in the catalytic activity.

The analysis of the experimental catalytic current densities was adjusted to the simple Koutecky-Levich (K-L) first order reaction equation (relationship between j^{-1} vs $w^{-1/2}$), without further need of additional terms:

$$\frac{1}{j} = \frac{1}{j_k} + \frac{1}{j_d} = \frac{1}{j_k} + \frac{1}{Bw^{1/2}} \tag{2}$$

Where j_k is the kinetic current density and B is related to the diffusion current density expressed as: $j_d = Bw^{1/2}$ and w is the angular frequency of rotation in revolutions per minute. The B parameter is defined as:

$$B = 0.2nFD^{2/3}v^{-1/6}C_{O2} \tag{3}$$

Where 0.2 is a constant used when *w* is expressed in revolutions per minute, *n* is the number of electrons transferred in the overall reduction process, *F* is the Faraday constant (96490 $Cmol^{-1}$), *D* is the diffusion coefficient of the molecular O_2 in 0.5 M H_2SO_4 (1.4 $x10^{-5}$ cm^2s^{-1}), *v* is the kinematic viscosity (0.01 cm^2s^{-1}) and C_{O2} is the concentration of molecular oxygen (1.1$x10^{-6}$ $molcm^{-3}$) [31]. A plot of j^{-1} vs $w^{-1/2}$ should give parallel straight lines for different potentials in mixed kinetic-diffusion controlled region, indicates that the number of electrons transferred per O_2 molecule and the active surface area for the reaction do not change significantly within the potential range studied. Figure 5 (b) and 6 (b), show the K-L plot of RuSe and RuMo to 40 h respectively. The linearity and parallelism of the lines in both systems, suggest that the oxygen reduction proceed via the overall four electrons transfer process indicating the complete reduction of O_2 to water formation, i.e., $O_2 + 4H^+ + 4e^- \rightarrow 2H_2O$. Parallelism of the straight line indicates that the number of electrons transferred per O_2 molecule and the active surface area for the reaction do not change significantly within the potential range studied. The experimental slope (B) of 7.60$x10^{-2}$ $mAcm^{-2}$ for RuSe and 7.62$x10^{-2}$ $mAcm^{-2}$ for RuMo are in agreement with the theoretical calculated value of 10.63 $x10^{-2}$ $mAcm^{-2}$ estimating for ORR of other Ru based compounds [10,32-35].

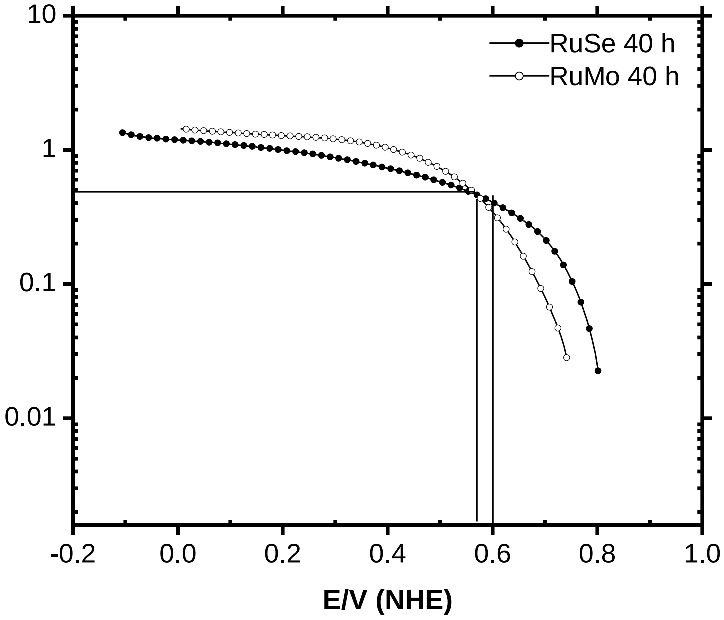

Figure 7. Mass transfer corrected Tafel plots for RuSe and RuMo at 40 h of milling, corresponding to the potential for attained 0.4 mA cm^{-2}.

The reaction order was evaluated further by plotting log *j* *vs* log ((1-*j*)/j_d) using data for polarization curves. As expected, the slop of the straight lines of the Figure 5 (c) y 6 (c) to RuSe y RuMo respectively, is close to one, confirming a first-order dependence on the kinetics, that corresponds to the transfer of the first electron of the catalysts to the molecule of oxygen adsorbed in the surface of the electrode, in agreement with the reaction: $(O_2)_{ads} + H^+ + e^- \rightarrow (HO_2)_{ads}$, being the rate determining step of the reduction reaction.

The Tafel plots were obtained after the measured currents were corrected for diffusion to give the kinetic currents in the mixed activation-diffusion region, calculated from:

$$j_k = \frac{jj_d}{j_d - j} \qquad (4)$$

Where $j_d/(j_d-j)$ is the mass transfer correction. The Tafel plots show a linear behavior in the mixed activation-difussion region and a deviation of the kinetic current occurs with higer slope at high current density.

Table 2. Kinetic parameters deduced for the oxygen reduction on RuSe, RuMo, RuW, RuSn catalysts to 20 and 40 h of milling in a 0.5 M H_2SO_4 solution.

ELECTROCATALYSTS	E_1=0 V/ENH	Reaction order	- b mVdec^{-1}	α	i_O mA cm^{-2}	n	E V/ENH at i=0.4mAcm^{-2}	η V
Ru-Se 20 h	0.77	1.3	129.08	0.459	1.82x10^{-6}	4	0.103	0.459
Ru-Se 40 h	0.80	1.0	109.13	0.542	4.10x10^{-6}	4	0.604	0.429
Ru-Mo 20 h	0.55	1.0	196.07	0.302	1.28 x 10^{-4}	4	0.407	0.679
Ru-Mo 40 h	0.70	1.0	134.23	0.441	9.55 x 10^{-6}	4	0.588	0.529
Ru-W 20 h	0.60	-	-	-	-	-	-	0.629
Ru-W 40 h	0.63	-	-	-	-	-	-	0.599
Ru-Sn 20 h	0.62	-	-	-	-	-	-	0.609
Ru-Sn 40 h	0.64	-	-	-	-	-	-	0.589

In all cases, the Tafel plots show a linear behavior in the mixed activation-diffusion region and a deviation of the kinetic currents are observed. For practical applications, is better to work at a fixed current density and rank the catalysts not in term of exchange current density and mainly in terms of the overpotential, so Figure 7 depicts the corresponding potential attained at 0.4 mAcm^{-2} for RuSe and RuMo (40 h milling). As one can see, RuSe has the lowest overpotential at this current density and would be considered as the best electrocatalyst for ORR in the acid electrolyte al 20 ºC. The kinetics parameters deduced for the ORR on all the catalyst at room temperature are presented in Table 2.

The intrinsic electrochemical properties for the ORR of the bimetallic surfaces have superior activity compared to ruthenium alone, which could be attributed to the bifunctional and electrical effects [36], in which the unique catalytic properties of each of the elements in the binary compound combine in a synergetic fashion to yield a more active surface than each of the elements alone, *i.e.*, the selenium acting as an oxygen adsorption site, promoting the electron transfer between the support (Vulcan carbon) and the catalytic center (Ru). This mechanism is thought to protect the catalyst from the formation of inactive ruthenium oxide, making the ruthenium-selenide base material stable against the corrosive environment within the fuel cell [37]. The molybdenum facilitates electron delocalization resulting a high conductivity [38].

3.2.2. Temperature dependence of the electrode kinetics of O_2 reduction

A study of temperature dependence of the electrode kinetic and mass transfer parameters is essential for the analysis of the influence of activation and diffusion controlled processes on the performance of fuel cells. The temperature dependence study was conducted in an oxygen saturated 0.5 M H_2SO_4 and temperature was varied from 293 to 333 K.

The charge transfer coefficients, α, considered as one of the parameters that allows to evaluate the mechanism of electrode reactions or to distinguish between different plausible mechanisms [39] and the exchange current density, j_o, were evaluated from the Tafel slope as a function of temperature, taking into account the reversible oxygen electrode potential, E_r, at each temperature [40]. The dependence of E_r on the temperature was evaluated using the value of ΔG^o at various temperatures from an equation reported by Lewis and Randall [41]:

$$\Delta G^0 = [-296.658 - 33.6T \ln T + 389.8T] \quad \text{J mol}^{-1} \tag{5}$$

$$E_r = \Delta G^0 / nF \tag{6}$$

ΔG^0 represents the free energy for the H_2-O_2 reaction producing liquid water and n number of electrons transferred to produce one mole of water (n=2).

The Tafel slopes are important to know the electrochemical reaction mechanisms with a linear dependence on temperature. The Tafel slopes were calculated using the following relationship:

$$b = \frac{dE}{d \log i} = -2.303 \frac{RT}{n\alpha F} \tag{7}$$

The Tafel plots at all temperatures show linear regions at low current density from which kinetic parameters were deduced. The electrode potential shift to more positive values and an increase of the catalytic current density is observed with raised temperature. This behavior is similar for RuSe and RuMo to 40 h of milling and it is attributed to an enhancement of the electrocatalytic kinetic reduction of the adsorbed oxygen with temperature. Figures 8 and 9 (a), show the temperature dependence of the mass transfer corrected Tafel coefficient for the oxygen reduction to RuSe and RuMo respectively, the Tafel slopes are temperature invariant with a constant slope of - 0.100 and -0.135 Vdec^{-1}, indicating that in the range of 293-333 K, the rate determining step in ORR is the first electron charge transfer, i.e., $(O_2)_{ads} + H^+ + e^- \rightarrow (HO_2)_{ads}$. The charge transfer coefficient, α, calculated from the Tafel slopes are plotted as a function of temperature in Figure 8, for RuSe slope, increases lineally with the absolute temperature ($d\alpha/dT$ = 5 x 10^{-4} K^{-1}) and the slope for RuMo electrocatalysts (Figure 9), increases lineally too with the absolute temperature, ($d\alpha/dT$ = 2 x 10^{-4} K^{-1}).

The finding that the transfer coefficient has a direct proportionality to temperature represents a significant feature.

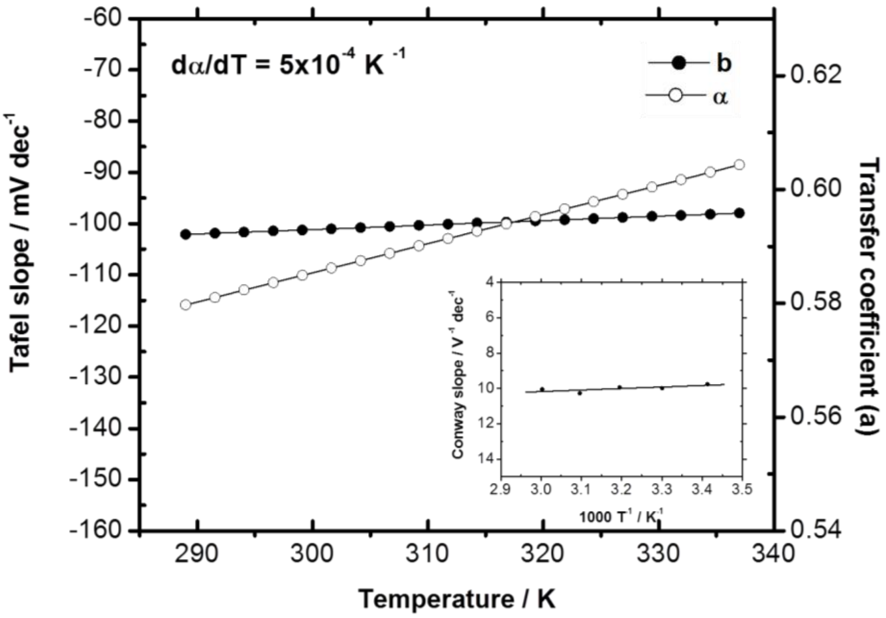

Figure 8. Tafel slope and transfer coefficient variation as a function of temperature for RuSe. Inset: Conway plot of the reciprocal of the Tafel slope against 1000/T.

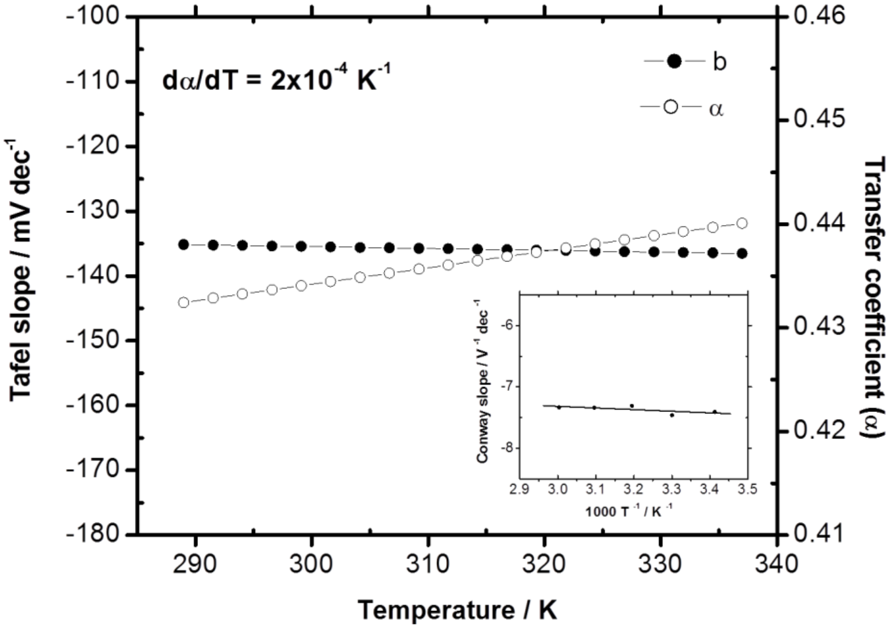

Figure 9. Tafel slope and transfer coefficient as a function of temperature for RuMo. Inset: Conway plot of the reciprocal of the Tafel slope against 1000/T.

Table 3. Kinetic parameters deduced of ORR on RuSe and RuMo catalysts in 0.5 M H_2SO_4 at different temperature.

Electrocatalysts	b_{prom} V dec^{-1}	$d\alpha/dT$ K^{-1}	$\alpha=\alpha H+T\alpha S$	$E^{\#}$ kJ mol^{-1}
RuSe	-0.100	$5x10^{-4}$	$-1.69x10^{-4} + 2.52x10^{-3}\ K^{-1}\ T$	34.93
RuMo	-0.136	$2x10^{-4}$	$-0.522x10^{-4} - 1.29x10^{-3}\ K^{-1}\ T$	49.29

The kinetic parameters deduced of ORR studies on RuSe and RuMo electrocatalysts in 0.5 M H_2SO_4 at different temperature are showing in Table 3. In general, the transfer coefficient (α) varies with the absolute temperature by the linear relationship:

$$\alpha = \alpha_H + T\alpha_S \qquad (8)$$

Where α_H is related to the change of electrochemical enthalpy of activation with electrode potential and α_S is related to the change of electrochemical entropy of activation with electrode potential [42]. According to this equation, the Tafel slopes of eq. (7) can be represented as:

$$b = -2.3\frac{RT}{(\alpha_H + T\alpha_S)F} \qquad (9)$$

Where α_H and α_S can be determined by plotting the Tafel slope reciprocal in function of the *T* reciprocal, named as Conway plot (inset Fig 8 and 9). From the slope and the intercept of this line, α_H and α_S are calculated for RuSe and RuMo as seen as Table 3.

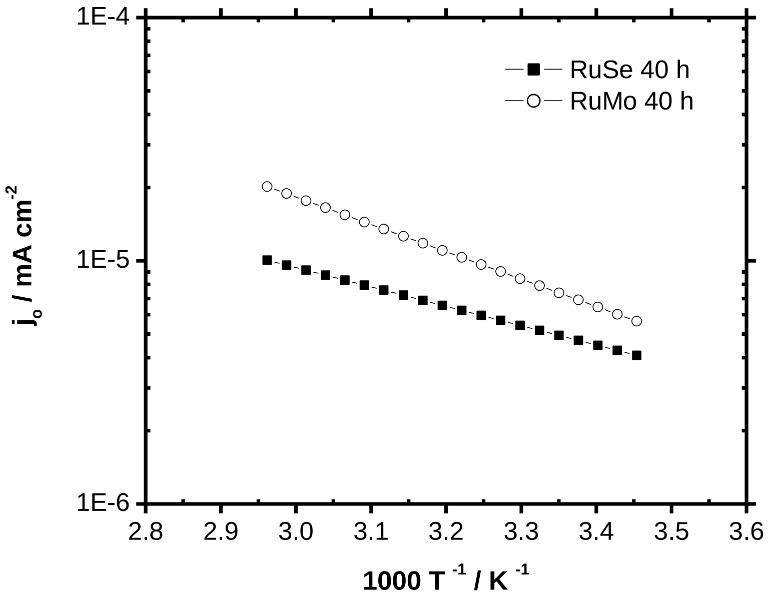

Figure 10. Electrochemical Arrhenius plot of the exchange current density at the reversible potential for ORR for RuSe electrode.

The low value of α_H in both electrocatalysts, suggests a negligible enthalpic contribution on the electrocatalysts behavior, therefore, the entropic contribution largely affects the final value of the global charge transfer. This behavior is common in the electrocatalysts that contain transition metals as active site [42-44].

The exchange current density (j_o), corresponding to each Tafel slope was calculated by extrapolating the potential to the E_r value at the operated cell temperature evaluated from eq. 9. The apparent activation energy, $E^{\#}$, was calculated from the Arrhenius slope represented by the relationship:

$$E^{\#} = 2.303R\left[\frac{d\log i_0}{d\left(1/t\right)}\right] \tag{10}$$

Figure 10, depicts the Arrhenius plots from the exchange current density. The apparent activation energy for RuSe and RuMo are 34.93 and 49.29 $\mathrm{KJmol^{-1}}$, respectively. These values are in the range of 30 - 80 $\mathrm{KJmol^{-1}}$ reported for ORR in acid media [3,45,46]. The apparent activation energy of RuSe is greater than RuMo, indicating that the energetically the ORR is favored on RuSe electrocatalyst. The apparent activation energy for RuSe and RuMo are shown in Table 3.

4. CONCLUSIONS

The present study demonstrates that mechanical alloying is an effective method for the preparation of nanometric RuSe, RuMo, RuW and RuSn electrocatalysts. The addition of a second material to Ru, improves the electrocatalytic activity toward the ORR by bifunctional and electronic effects. The physical characterization of RuSe catalysts to 40 h of milling time, showed the formation of $FeSe_2$, Fe_2O_3, Ru and Se mixture of phases; a RuMo solid solution, both electrocatalysts with granular morphology; a $RuSe_2$ intermetallic and a Ru_3W_2 intermetallic with irregular morphology. The electrochemical characterization shows that the materials studied are active towards the ORR with the exception of RuW and RuSn. The ORR proceeds predominantly with four electrons transfer to water formation with a first order reaction respect the oxygen concentration. The Tafel slope and transfer coefficient values show the influence of the Ru intrinsic characteristics used by active center, but in the exchange current and the activation energy, there are greater influences of the second transition metal. The temperature effect on the electrochemical parameters indicates that the Tafel slope is temperature invariant while the transfer coefficient shows important absolute temperature dependence. In RuSe and RuMo electrocatalysts, the enthalpic contribution is the determining factor for the electrocatalytic activity of this reaction. The apparent activation energy values are presented in following order: RuSe > RuMo. The ORR activity shows a significant relationship with the crystallite size. The electrocatalytic efficiency order of the materials studies is RuSe > RuMo > RuSn > RuSn to 40 h of milling.

ACKNOWLEDGEMENTS

A. Ezeta-Mejía is grateful for her postgraduate fellowship from CONACYT and SIP-IPN. The authors are also grateful for the financial support from the SIP 2009-0561 project and SNI-CONACYT.

References

1. D.C. Martínez-Casillas, G. Vázquez-Huerta, J.F. Pérez-Robles, O. Solorza Feria, *J. Power Sources.* 196 (2011) 4468.
2. W. Jensen, O. Winther Jensen, M. Forsyth, D.R. MacFarlane, *Science.* 321 (2008) 671.
3. K. Kinoshita, Electrochemical Oxygen Technology, Willey, New York (1992).
4. T. Maiyalagan, S. Pasupathi, *Mat. Sci. Forum*, 657 (2010) 143.
5. P. He, M. Lefévre, G. Faubert, J.P. Dodelet, *J. New Mater. Electrochem. Syst*. 2 (1999) 243.
6. M. Lefévre, J.P. Dodelet, P. Bertrand, *J. Phys. Chem*. B 104 (2000) 11238.
7. M. Bron, S. Fiechter, M. Hilgendorff, P. Bogdanoff, *J. Appl. Electrochem*. 32 (2002) 211.
8. S. Durón, R. Rivera Noriega, M.A. Leyva, P. Nkeng, G. Poillerat, O. Solorza-Feria, *J. Solid State Electrochem.* 4 (2000) 7.
9. R.G. González-Huerta, A. Guzmán-Guzmán, O. Solorza-Feria, *Int. J. Hydrogen Energy*, 35 (2010)12115.
10. H. Tributsch, M. Bron, M. Hilgendorff, H. Schulenburg, I. Dorbandt, V. Eyert, P. Bogdanoff, S. Fiechter, *J. Appl. Electrochem*. 31 (2001) 739.
11. F. Dassenoy, W. Vogel, N. Alonso Vante, *J. Phys. Chem*. B 106 (2002) 12152.
12. R. González Cruz, O. Solorza Feria, *J. Solid State Electrochem*. 7 (2003) 289.
13. V. Le Rhun, N. Alonso Vante. *J. New Mater. Electrochem. Syst*. 3 (2000) 331.
14. L. Mao, D. Zhang, T. Sotomura, K. Nakatsu, N. Koshiba, T. Ohsaka, *Electrochim. Acta*. 48 (2003) 1015.
15. M. Bron, P. Bogdanoff, S. Fiechter, M. Hilgendorff, J. Radnik, I. Dorbandt, H. Schulenburg, H. Tributsch, *J. Electroanal. Chem.* 517 (2001) 85.
16. M. Hilgendorff, K. Diesner, H. Schulenburg, P. Bogdanoff, M. Bron, S. Fiechter, *J. New Mater. Electrochem. Syst*. 5 (2002) 71.
17. T.J. Schmidt, U.A. Paulus, H.A. Gasteiger, N. Alonso Vante, R.J. Behm, *J. Electrochem. Soc*. 147 (2000) 2620.
18. H. Cheng, W. Yuan, K. Scott, *Electrochim. Acta*. 52 (2006) 466.
19. K.S. Nagabhushana, E. Dinjus, H. Bönnemann, V. Zaikovskii, C. Hartnig, G. Ehl, I. Dorbandt, S. Fiechter, P. Bogdanoff, *J. Appl Electrochem*. 37 (2007) 515.
20. M. Montiel, S. García Rodríguez, P. Hernández Fernández, R. Díaz, S. Rojas, J.L. Fierro, E. Fatás, P. Ocón, *J. Power Sources*. 195 (2010) 2478.
21. K. Suárez-Alcántara, O. Solorza-Feria, *Electrochim. Acta*. 53-15 (2008) 4981.
22. M.T.M. Koper, *Surface Science*. 548 (2004) 1.
23. L. Xiong, T. He, *Electrochem. Comun*. 8 (2006) 1671.148.
24. B.D. Cullity, Elements of X-Ray Difracction, Addison-Wesley Publishing Company, INC., USA (1978).
25. M.R. Paruchuri, D.L. Zhang, T.B. Massalski, *Mater. Sci. Eng*. A 174 (1994) 119.
26. P. Sotelo Mazón, R.G. González Huerta, J.G. Cabañas Moreno, O. Solorza-Feria, *Int. J. Electrochem.Sci.* 2 (2007) 523.
27. C.C. Koch, Annu. *Rev. Mater. Sci*. 19 (1989) 121.
28. M.Bron, P. Bogdanoff, S. Fiechter, I. Dorbandt, M. Hilgendorff, H. Schulenburg, H. Tributsch, *J. Electroanal Chemistry.* 500 (2001) 510.
29. S. Hadzi Jordanov, H. Angerstein Kozlowska, M. Vuckovic, B.E. Conway, J. Phys. Chem. 81 (1977) 2271.

30. U.A. Paulus, T.J. Schmidt, H.A. Gasteiger, R.J. Behm, *J. Electroanal. Chem*. 495 (2001) 134.
31. C. Coutanceau, P. Crouigneau, J.M. Léger, C. Lamy, *J. Electroanal. Chem*. 379 (1994) 389.
32. R.G. González Huerta, R. González Cruz, S. Citalán Cigarroa, C. Montero Ocampo, O. Solorza Feria, *J. New Mat. Electrochem. Systems*. 8 (2005) 15.
33. R. González Cruz, O. Solorza Feria, *J. Sol. State Electrochem*. 7 (2003) 289.
34. T.J. Schmidt, U.A. Paulus, H. Gasteiger, N. Alonso Vante, R.J. Behm, *J. Electrochem. Soc*. 147 (2000) 2620.
35. J. Prakash, H. Joachin, *Electrochim. Acta*. 45 (2000) 2289.
36. M.T.M. Koper, *Surface Science*. 548 (2004) 1.
37. K. Suárez Alcántara, O. Solorza Feria, *Electrochim. Acta*.. 53 (2008) 4981.
38. N. Alonso Vante, W. Jaegermann, H. Trbutsch, W. Honle, K. Yvon, *J. Am. Chem. Soc*. 109 (1987) 3251.
39. S. Durón. PhD. Thesis, Cinvestav-IPN, México (2000).
40. A. Parthasaranthy, S. Srinivasan, A.J. Appleby, C.R. Martin, *J. Electrochem Soc*. 139 (1992) 2530.
41. G. Lewis, M. Randall, International critical tables. Vol. 7. Mc Graw Hill, New York (1930).
42. A. Damjanovic, *J. Electroanal. Chem*. 355 (1993) 57.
43. B.E. Conway, Modern Aspects of Electrochemistry. Vol 16. Cap. 2. B.E. Conway, R.E. White, J.O´M. Brockris. Ede. Plenum Press. N.Y. USA (1985).
44. B.E Conway, D.F. Tessier, D.P. Wilkinson, *J. Electrochem. So*c. 136 (9) (1989) 2486.
45. R.G. González Huerta, R. González Cruz, C. Montero Ocampo, J. Chávez Carvallar, O. Solorza Feria, *J. New Mater. Electrochem. Syst*. 8 (2005) 15.
46. K. Suárez Alcántara, A. Rodríguez Castellanos, R. Dante, O. Solorza-Feria, *J. Power Sources*. 157 (2006) 114.